Provided for non-commercial research and education use.
Not for reproduction, distribution or commercial use.

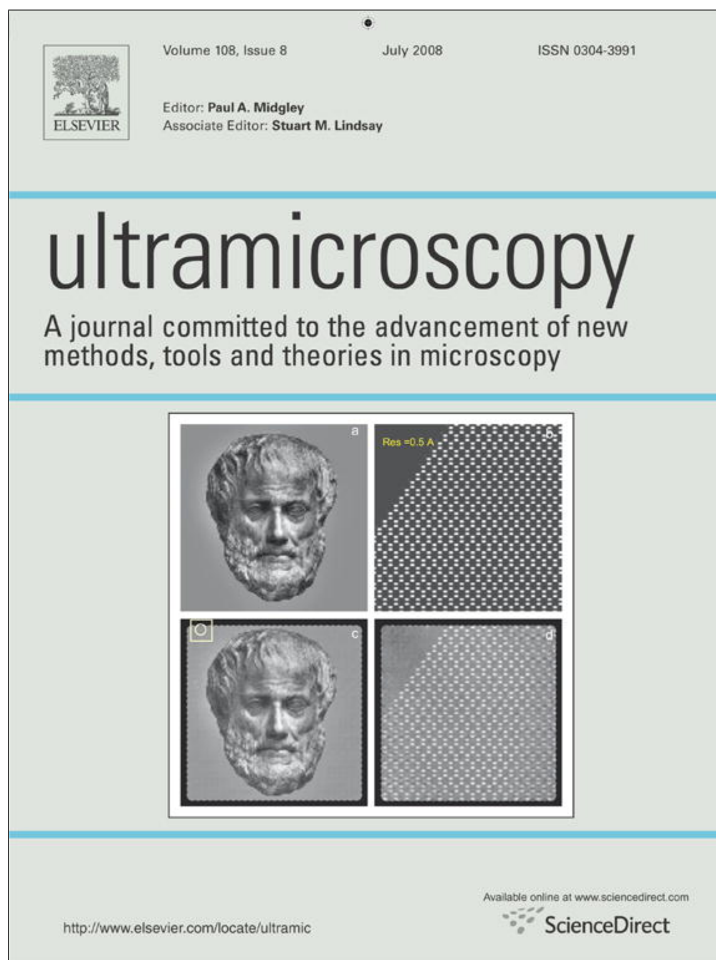

This article appeared in a journal published by Elsevier. The attached copy is furnished to the author for internal non-commercial research and education use, including for instruction at the authors institution and sharing with colleagues.

Other uses, including reproduction and distribution, or selling or licensing copies, or posting to personal, institutional or third party websites are prohibited.

In most cases authors are permitted to post their version of the article (e.g. in Word or Tex form) to their personal website or institutional repository. Authors requiring further information regarding Elsevier's archiving and manuscript policies are encouraged to visit:

http://www.elsevier.com/copyright

Author's personal copy

ELSEVIER

Available online at www.sciencedirect.com
ScienceDirect

Ultramicroscopy 108 (2008) 718–726

ultramicroscopy

www.elsevier.com/locate/ultramic

Effects of tilt on high-resolution ADF-STEM imaging

S.E. Maccagnano-Zacher, K.A. Mkhoyan*, E.J. Kirkland, J. Silcox

School of Applied and Engineering Physics, Cornell University, Ithaca, NY 14853, USA

Received 19 July 2007; received in revised form 24 October 2007; accepted 2 November 2007

Abstract

A study of the effects of small-angle specimen tilt on high-resolution annular dark field images was carried out for scanning transmission electron microscopes with uncorrected and aberration-corrected probes using multislice simulations. The results indicate that even in the cases of specimen tilts of the order of 1° a factor of 2 reduction in the contrast of the high-resolution image should be expected. The effect holds for different orientations of the crystal. Calculations also indicate that as the tilted specimen gets thicker the contrast reduction increases. Images simulated with a low-angle annular dark field detector show that tilt effects are more pronounced in this case and suggest that these low-angle detectors can be used to correct specimen tilt during scanning transmission electron microscopes operation.

© 2007 Elsevier B.V. All rights reserved.

PACS: 68.37.Ma; 34.80.Bm; 61.85.+p; 61.72.uf

Keywords: STEM; Tilt; ADF imaging; Aberration-correction; Si

1. Introduction

Advances in spherical aberration corrected conventional and scanning transmission electron microscopes ((S)TEMs) [1,2], where probe sizes reach below 1 Å, allow imaging of crystalline specimens with atomic resolution routinely [3,4]. However, a full understanding of all the processes that create the intensity variations in the high-resolution images (bright spots in the locations of the atomic columns on the dark background) is still an unsolved problem. The problem exists for TEM bright field as well as for STEM annular dark field (ADF) images. For conventional TEMs, the discrepancy between the contrasts obtained from theoretically modeled and experimentally recorded images, known as the "Stobbs factor", has been a subject of extensive research for many years. A series of papers by Boothroyd and co-authors discussing possible explanations deserve close attention [5–7].

While in early ADF-STEM studies the effects of phonon scattering [8] and plasmon generation [9,10] caused by inelastic scattering of the probe electrons have been discussed as the primary factors contributing to contrast reduction in the experimentally recorded high-resolution images, the contributions from the specimen tilt have not been studied in sufficient detail. In (S)TEM experiments a misalignment of the specimens of several milliradians from the targeted zone axis orientation can be present and could go unnoticed. In cases of thin specimens where the tilt is not large (less than a few degrees) high-resolution imaging of the atomic columns is still possible. However, with tilt the channeling of the incident electron beam will be affected and, therefore, some reduction in contrast is expected. Some discussions of the tilt effects on ADF-STEM imaging have been reported previously by a Cornell group [11,12], Plamann and Hytch [13], Yamazaki et al. [14] and Wang et al. [15]

In an earlier paper Yu et al. [12] reported experimentally recorded ADF images of Si specimens at high-angle tilt using 200 kV, uncorrected STEM and compared them with multislice simulations. The primary point of that paper was to record the serious drop in intensity within a couple of degrees or so away from zone axis. In this paper we explore the effects of even smaller specimen tilts on high-resolution

*Corresponding author. Tel.: +1 607 255 0649.
E-mail address: kam55@cornell.edu (K.A. Mkhoyan).

0304-3991/$ - see front matter © 2007 Elsevier B.V. All rights reserved.
doi:10.1016/j.ultramic.2007.11.003

Author's personal copy

ADF-STEM imaging with an emphasis on the visibility of the atomic columns, i.e., contrast, also using a computational multislice method [16]. The method has been successfully implemented to understand experimental observations of the changes in the contrast of the crystal lattice fringes as a function of defocus [17,18], and convergent-beam electron diffraction (CBED) patterns [8]. It has also been used to describe the effects of beam broadening in GaN/AlN quantum wells [19].

2. Multislice ADF-STEM simulations

The algorithm for all calculations of ADF-STEM images is based on the multislice method [16]. In this method a STEM focused electron probe is generated using typical experimental parameters. Then the incident electron beam is propagated through the entire thickness of the specimen by alternately passing through thin (one atomic layer) layers of the specimen and propagating between the layers. The ADF intensity is then calculated by summing up all of the electrons that are elastically scattered from the atoms of the specimen into the conical solid angle of the ADF detector. The final image is generated by scanning the probe position across the area of the model specimen [20]. The thermal vibrations of the atoms (or phonons) are included in the calculation by randomly displacing atoms from their lattice sites using a Gaussian distribution function with the corresponding Debye–Waller factors [8] for each atom species.

All of the ADF-STEM image simulations presented in this paper were carried out using Si crystal test specimens. The sizes of the Si supercells used in the calculations were $27.15 \times 26.88\,\text{Å}^2$ for the [1 1 0] oriented sample and 27.15×27.15 and $26.88 \times 26.60\,\text{Å}^2$ for the [1 0 0] and [1 1 1] oriented samples, respectively. The images were obtained by scanning the probe over an $11 \times 8\,\text{Å}^2$ area in the center of the supercell with 65×47 pixels. The following slice thicknesses were used in all simulations: 1.920 Å in the crystals aligned along [1 1 0] and 3.135 and 1.357 Å for the crystals along [1 0 0] and [1 1 1], respectively. All calculated ADF intensities are normalized to a total intensity of the incident beam. Because the incident probe intensities in all calculations are kept the same, they are all normalized to the same value. This normalization, identical to a single incident electron, is essential for quantitative comparison of different ADF images. In simulations the x and y tilts of the crystal were introduced by rotating the crystal around the y and x axes, respectively. The diagram of the x–y geometry of the Si crystal when it is oriented along the [110] orientation is presented in Fig. 1. The details of the introduction of the tilt in multislice can be found in Ref. [20].

Two STEM probes were considered in this study. First, a $\simeq 2\,\text{Å}$ probe (uncorrected for spherical aberrations) was generated using the following electron optical parameters: 100 kV acceleration voltage, spherical aberration of $C_s = 1.3\,\text{mm}$, objective angle of $\alpha = 11.4\,\text{mrad}$, and defocus of $\Delta f = 850\,\text{Å}$. While these numbers are typical for the Cornell STEM, they are also comparable to the optical conditions of other STEMs with similar resolutions. Second, a new probe of $\simeq 0.8\,\text{Å}$ was created using corrections to the axial aberrations up to 5th order: acceleration voltage of 100 kV, $C_{s(3)} = -0.015\,\text{mm}$, $C_5 = 10\,\text{mm}$, objective angle of $\alpha = 25\,\text{mrad}$, and defocus of $\Delta f = -30\,\text{Å}$ [21]. The contributions of the chromatic aberration are not included in these calculations. The profiles of these two probes are presented in Fig. 2. Both probes have the same total intensity. Images were calculated using 54 and 340 mrads inner and outer angles for the ADF detector. In all simulations presented here the beam was focused on the entry surface of the specimen [21].

Though in some standard definitions of contrast an ADF image of amorphous material would have value, the

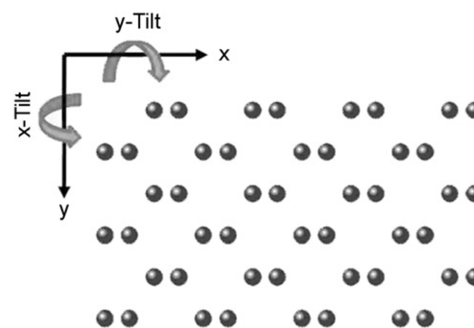

Fig. 1. Schematic diagram describing tilt axes and directions used here relative to a Si crystal oriented along the [1 1 0] crystallographic direction.

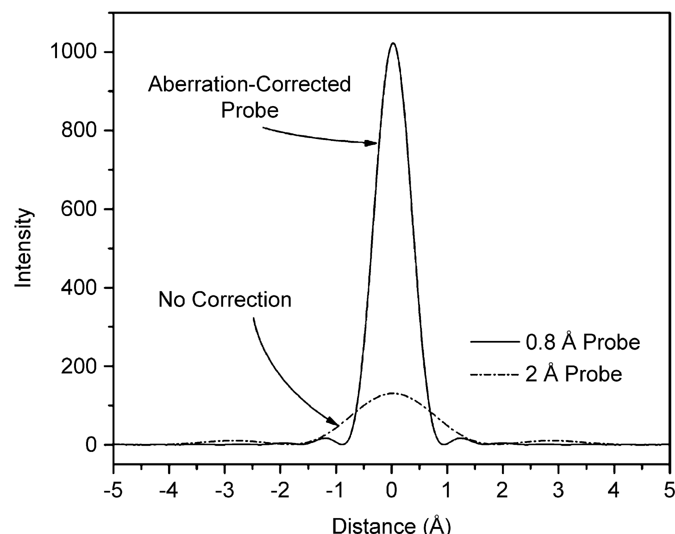

Fig. 2. Line profiles of the two STEM probes used in this study. Uncorrected 2 Å and aberration-corrected 0.8 Å probes were generated with the following optical parameters: uncorrected probe: $E_0 = 100\,\text{kV}$, $C_s = 1.3\,\text{mm}$, $\alpha_{obj} = 11.4\,\text{mrad}$, and $\Delta f = 850\,\text{Å}$, and aberration-corrected probe: $E_0 = 100\,\text{kV}$, $C_{s(3)} = -0.015\,\text{mm}$, $C_5 = 10\,\text{mm}$, $\alpha_{obj} = 25\,\text{mrad}$, and $\Delta f = -30\,\text{Å}$. These two probes are normalized to the same total intensity. From Ref. [21].

Author's personal copy

image would not have any lattice fringes or periodic intensity indicating the presence of a crystalline structure. Since this paper is concerned with quantifying the visibility of the crystal lattice in an image, we have chosen the following definition for contrast so that its value will be near zero when there is no visibility of atomic columns in the image [21]:

$$C = \frac{I_{max} - I_{min}}{I_{mean}}, \qquad (1)$$

where I_{max} is the mean value of the maximum intensity spots of an ADF crystal lattice image (on the atomic columns), I_{min} is the mean value of the minimum intensity spots of an ADF crystal lattice image (between the atomic columns), and I_{mean} is the mean intensity value of the entire ADF image.

3. Results

First, images of the crystal lattice of Si tilted about the [1 1 0] crystallographic orientation were simulated using a 2 Å probe. The crystal was tilted in 3 mrad steps around the x- and the y-axes (see Fig. 1). The crystal thickness in these calculations was 250 Å. An array of these images is shown in Fig. 3(a). Each image in the array is normalized to the incident beam, so the decrease in intensity of the atomic columns is more readily perceived. This decrease of intensity of Si atomic columns in high-angle ADF (HAADF) detectors for a $\simeq$ 2 Å probe has been also noted by Yu et al. [12]. Fig. 3(a) is similar to what a microscope operator would observe if they were lucky enough to find a variation of tilt of 1° within the microscope field of view and reflects these [12] intensity measurements. In comparison, Fig. 3(b) shows the same simulated data reflected in Fig. 3(a), but now the images in this figure are individually rescaled to fill the available grayscale internal to each image. This illustrates the change in appearance of the crystal lattice viewed by the microscope operator as they move about and image the sample. Therefore, for lattice images, changes in appearance of the lattice images and not intensity will be the first indication that the sample has been tilted from on-axis orientation. It is interesting to note from Fig. 3(b) that even with a relatively large tilt of 15 mrad in x and y, the crystal lattice is still visible. In Fig. 3(b) the images with large single-axis tilt show an increase in the separation of the bright spots which may seem to indicate increased resolution but in reality it is a degradation in the imaging the dumbbell columns due to distortion from the tilt. At a more conservative tilt of 12 mrad in x and y, the crystal lattice image is one that appears to be "on axis" even though it is actually over 2/3 of a degree off the [1 1 0] axis in both the x- and y-axes. As mentioned previously, the images in Fig. 3(b) are scaled to fill the available grayscale and, therefore, for quantitative analysis the actual values of the ADF intensities are required. Fig. 4 shows the line scans across the simulated images whose intensities have not been rescaled. These line scans show a decrease of the highest intensity on the atom columns with increased tilt of the crystal, and very little change of the low intensity between the columns.

The values of the contrast (1) are also calculated for each image and the results are plotted in Fig. 5. The graph shows that the contrast decreases by about 60% and 30% when the crystal is tilted 15 mrad along the y- and x-axes. The maximum contrast reduction for a 15 mrad tilt angle occurs when only the y-axis is tilted. The contrast reduction seems to have some unexpected oscillatory behavior as the tilt increases. Fig. 5 shows that as the sample is tilted from the [1 1 0] orientation the contrast of the image reduces by a factor of 2 despite a strong visibility of the atomic columns in the image.

ADF images of the same Si crystal were also simulated using an aberration-corrected 0.8 Å probe. Here again 3 mrad tilt steps were used around the x- and y-axes. The resulting array of the ADF images is shown in Fig. 6. Similar to the case with 2 Å probe, the crystal lattice is

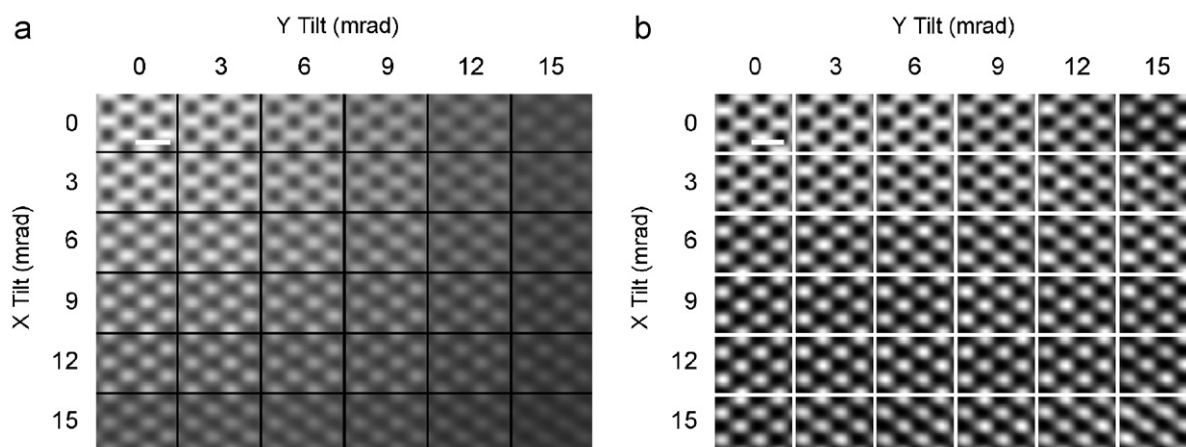

Fig. 3. Simulated ADF-STEM images of 250 Å thick crystal silicon specimens at different tilts. A 2 Å probe was used and the crystal was tilted around the [1 1 0] crystallographic orientation.The specimen tilt angles along x- and y-axes are indicated. (a) All images are normalized to the incident beam. (b) All images are scaled to fill the available grayscale. For both image (a) and (b), spots of bright intensity indicate location of atomic dumbbells and scale bars are 5 Å.

Author's personal copy

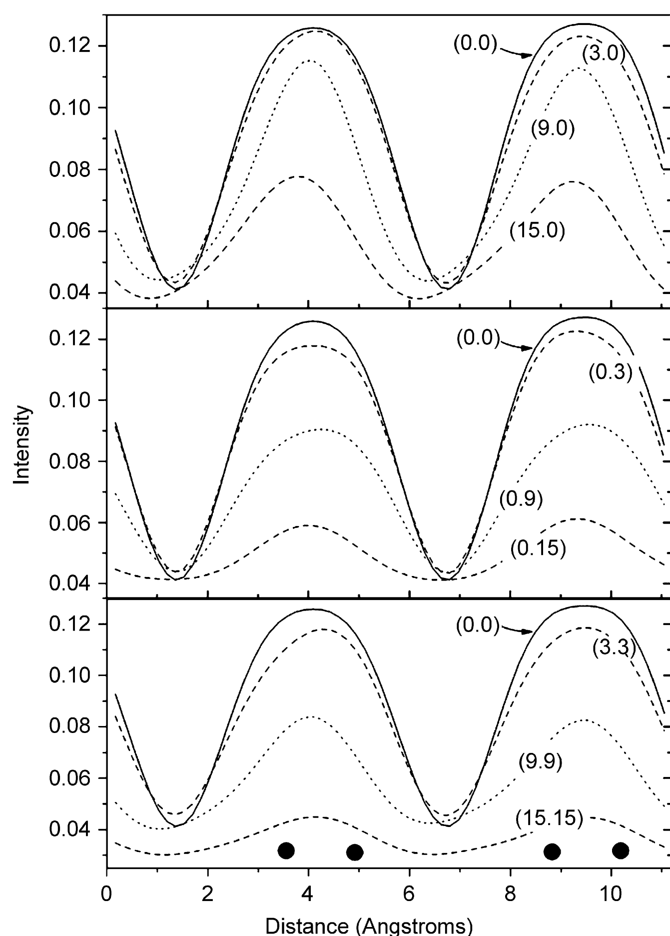

Fig. 4. Line scans from simulated ADF-STEM images of Si oriented along the [1 1 0] direction at different tilt angles calculated using a 2 Å probe and taken across the dumbbells. The tilt angles are given in brackets (x,y). The positions of atomic columns are indicated with black dots.

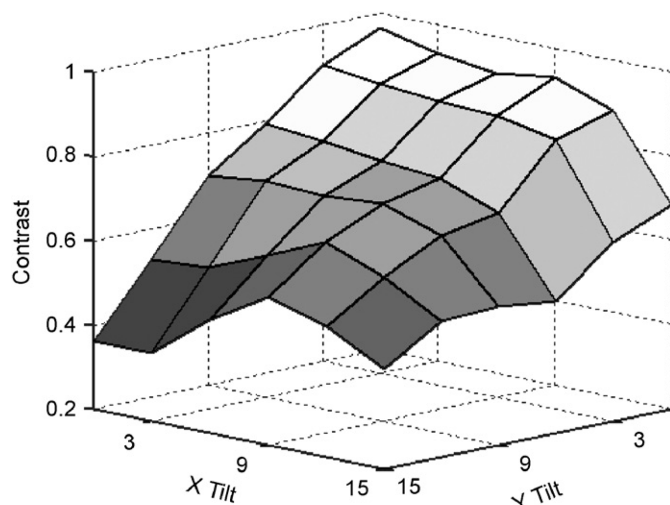

Fig. 5. The values of the contrast calculated from ADF-STEM images of a Si specimen simulated at different tilt angles around the [1 1 0] crystallographic orientation with a 2 Å probe.

visible throughout the tilt series. With the smaller probe there is very little discernible difference between the on-axis case and the largest tilt case. This was also observed

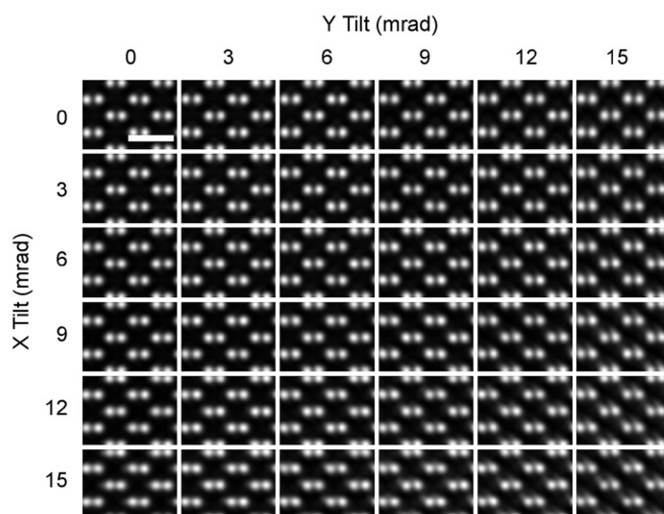

Fig. 6. Simulated ADF-STEM images of 250 Å thick crystal silicon specimens at different tilts. A 0.8 Å probe was used and the crystal was tilted around the [1 1 0] crystallographic orientation. The specimen tilt angles along x- and y-axes are indicated. All images are scaled to fill the available grayscale. White spots are atomic columns. The scale bar is 5 Å.

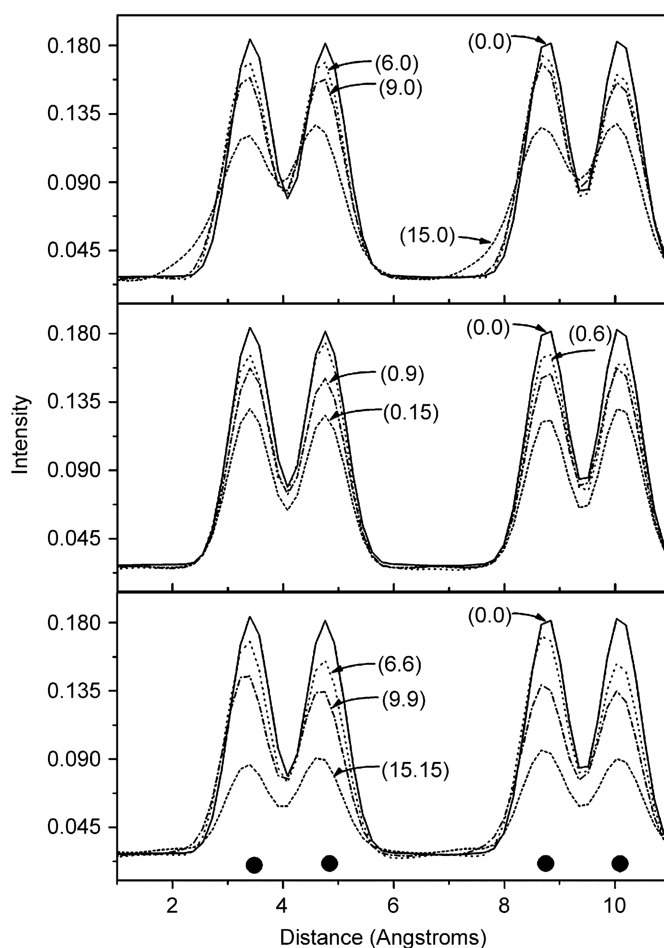

Fig. 7. Line scans from simulated ADF-STEM images of Si oriented along the [1 1 0] direction at different tilt angles calculated using a 0.8 Å probe and taken across the dumbbells. The tilt angles are given in brackets (x,y). The positions of atomic columns are indicated with black dots.

Author's personal copy

experimentally by Wang et al. [15]. Linescans from several of these images showing the actual values of the ADF intensities are presented in Fig. 7. The intensity of the bright spots, whose locations correspond to the positions of the atomic columns in an untilted crystal, is seen to decrease significantly as the tilt increases, decreasing to over half its value with a 15 mrad tilt in both axes. And again, as in the non-corrected probe case, the low intensity between the atomic columns does not change discernibly. The contrast values for all tilts are also calculated and the results are plotted in Fig. 8. This graph shows a much more regular reduction of contrast with an increase of tilt than the uncorrected probe, exhibiting no oscillations in contrast but instead reducing monotonically as the tilt increases. The highest tilt (15,15) creates an image with contrast almost half that of the untilted image.

The visibility of the atomic columns in the ADF images is sensitive to the channeling of the incident electron beam that propagates through the specimen along the atomic columns. The crystal orientation, specimen thickness and types of atomic species present in the sample are known to be critical factors that can significantly alter the beam channeling. In the next sections we discuss the effects of some of these factors that might occur in combination with and in the presence of tilt.

3.1. Different crystallographic orientations

A set of high-resolution ADF images of the Si specimens were calculated with the crystal oriented along the two other major crystallographic orientations: [1 0 0] and [1 1 1]. Images for 250 Å thick specimens were calculated for the aberration-corrected 0.8 Å probe while the crystal was on-axis and tilted off-axis in increments of 6 mrad around the *x*- and *y*-axes. Fig. 9 shows two arrays of images of these tilt series around [1 1 0] and [1 1 1] orientations. In both cases the crystal lattice is clearly visible even at the tilt of about 12 mrad. The values of the contrast calculated for both orientations are summarized in Table 1. As in the case near the [1 1 0] orientation, significant reduction of contrast

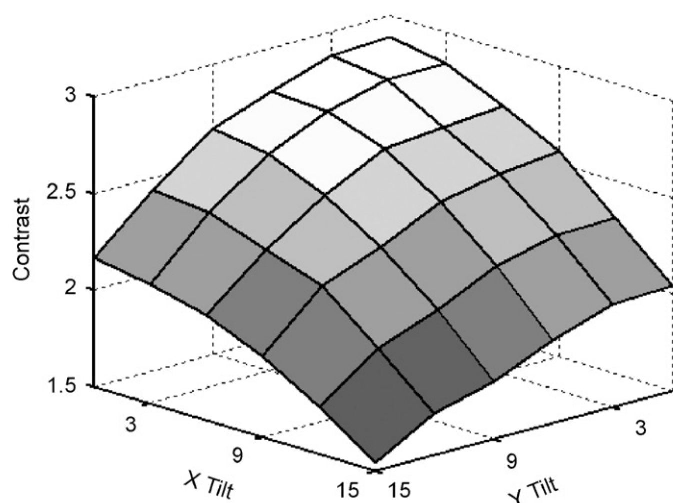

Fig. 8. The values of the contrast calculated from ADF-STEM images of a Si specimen simulated at different tilt angles around the [1 1 0] crystallographic orientation with a 0.8 Å probe.

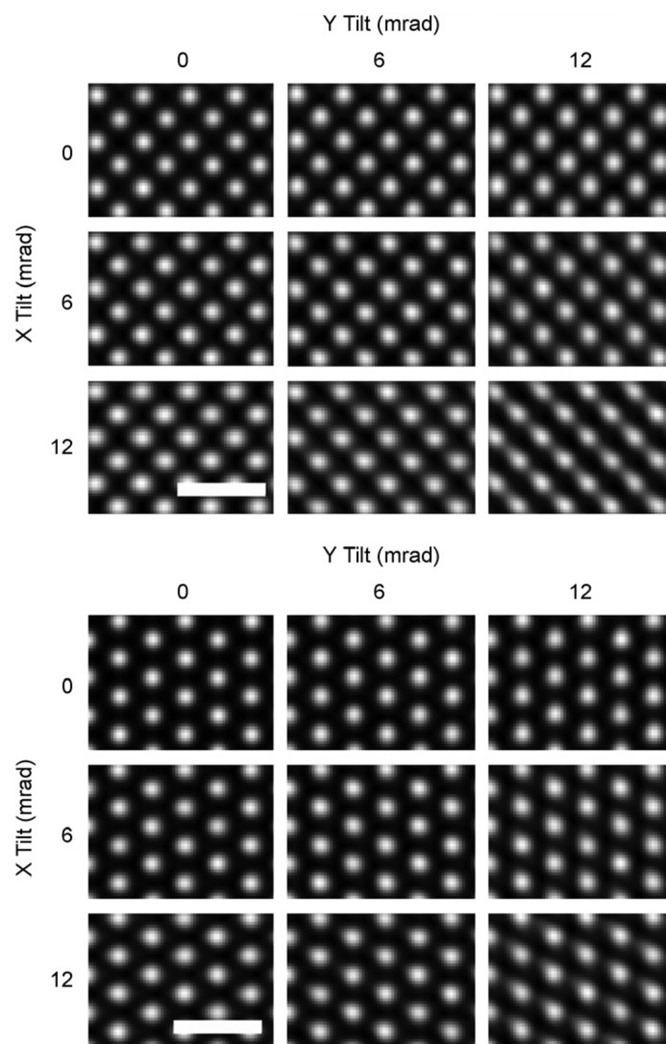

Fig. 9. Simulated ADF-STEM images of 250 Å thick crystal silicon specimens at different tilts. A 0.8 Å probe was used and the crystal was tilted around the [1 0 0] (top) and [1 1 1] (bottom) crystallographic orientations. The specimen tilt angles along *x*- and *y*-axes are indicated. All images are scaled to fill the available grayscale. White spots are atomic columns. The scale bar is 5 Å.

Table 1
Contrast values for a 250 Å thick Si specimen calculated from simulated ADF-STEM images using a 0.8 Å probe. Tilts are around [1 0 0]/[1 1 1] orientations

	Y Tilt (mrad)		
X Tilt (mrad)	0	6	12
0	1.536/1.896	1.435/1.816	1.243/1.458
6	1.429/1.753	1.348/1.649	1.165/1.365
12	1.219/1.488	1.166/1.383	0.890/1.105

Author's personal copy

is observed when the crystal is tilted off-axis from the [1 0 0] and [1 1 1] orientations. For example, at a 12 mrad tilt in both x and y the atomic contrast of the high-resolution ADF images decreases by a factor of 0.6.

3.2. Different specimen thicknesses

A series of ADF-STEM images of Si crystals was simulated for thicknesses from 50 to 750 Å with 50 Å steps. For enhancement of the effects the specimen was tilted to 15 mrad (or $\approx 1°$) off of the [1 1 0] orientation around both the x- and y-axes. For a 750 Å-thick sample under these tilt conditions the top and bottom atoms of atomic columns in Si are shifted with respect to one another in the x–y plane by 11.2 Å, leading one to expect dramatic changes in the tilted ADF images. As before, two STEM probes were considered here: the 2 Å probe and the aberration-corrected 0.8 Å probe. Eight of these simulated ADF images for both probes are presented in Fig. 10. Surprisingly, as can be seen from Fig. 10, even for a 750 Å thick specimen, atomic columns are still visible. The positions of the bright spots correspond to the positions of the top atoms in the columns.

For detailed analysis the contrast of all simulated ADF images was calculated and the values of C are plotted as a function of thickness in Fig. 11(a). In addition, the values of the ADF intensities of the bright spots corresponding to the position of the atomic columns and dim spots (the spots in between the columns with the smallest intensity) as well as the mean intensity values of the images are presented in Fig. 11(b). The intensities of the bright spots increase with thickness as does the mean intensity of the image, however, the contrast drops as thickness increases. The contrast reduces fairly quickly for specimens with thicknesses from 50 to 150 Å and then decreases at a slower rate up to the final thickness of 750 Å. This type of dependence of the contrast to the thickness was observed for both probe sizes.

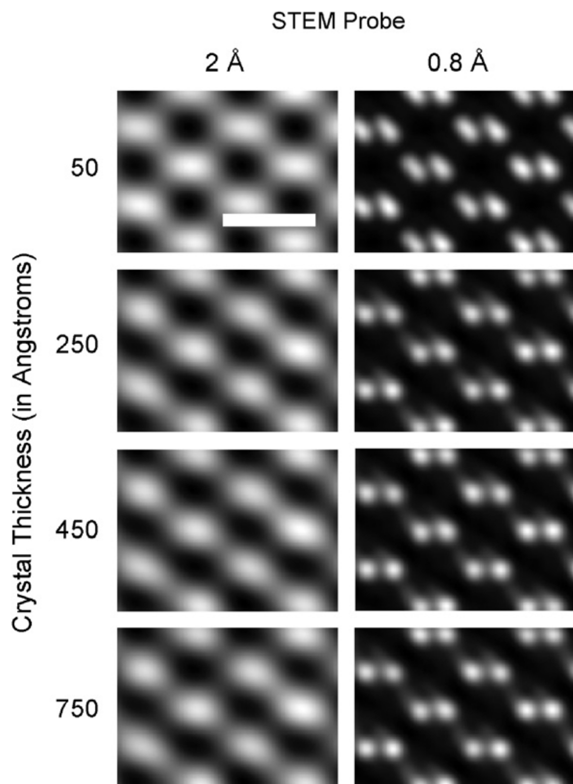

Fig. 10. Simulated ADF-STEM images of crystal silicon specimens at different thicknesses with (15,15) mrad tilt off of the [1 1 0] crystallographic orientation. Left column is calculated with a 2 Å probe and right column with a 0.8 Å probe. All images are scaled to fill the available grayscale. The scale bar is 5 Å.

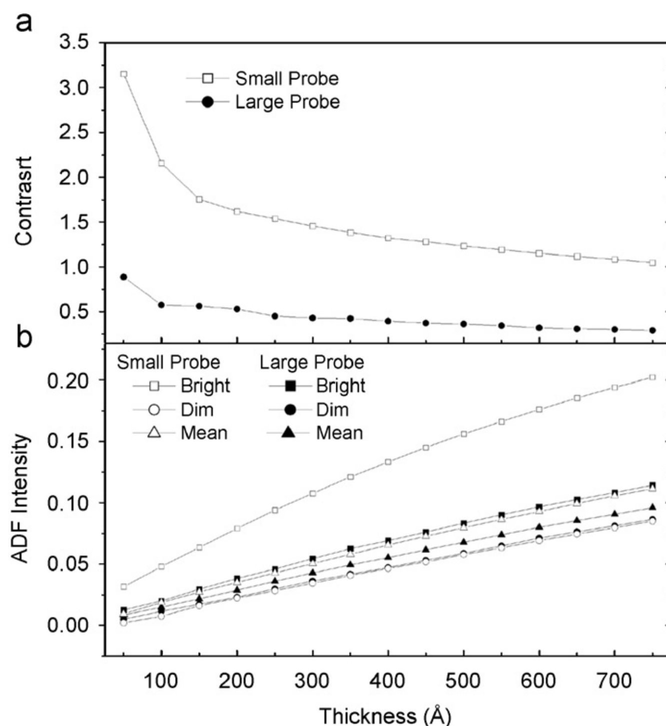

Fig. 11. (a) Dependence of the ADF image contrast on specimen thickness as calculated for a Si specimen tilted (15,15) mrads off of the [1 1 0] crystallographic orientation. Uncorrected and aberration-corrected probes are considered. (b) The actual intensities from the brightest and dimmest spots and mean intensities of the ADF images as a function of thickness.

3.3. Different ADF detectors

All of the ADF-STEM simulated images presented to this point have been calculated using an ADF detector with 54–330 mrad inner–outer angles. The sensitivity of the ADF signal to the detector geometry and in particular to the inner angle has already been studied in detail and as a result some STEMs are now equipped with double ADF detectors which record simultaneous images. The nested detectors consist of a low-angle ADF (LAADF) detector that typically has 25–50 mrad inner–outer angles and an HAADF detector that collects electrons scattered into 50–250 mrad conical solid angle [22]. HAADF images are expected to form images of the specimen with primarily incoherently scattered electrons while the LAADF images tend to have a combination of incoherently and coherently

Author's personal copy

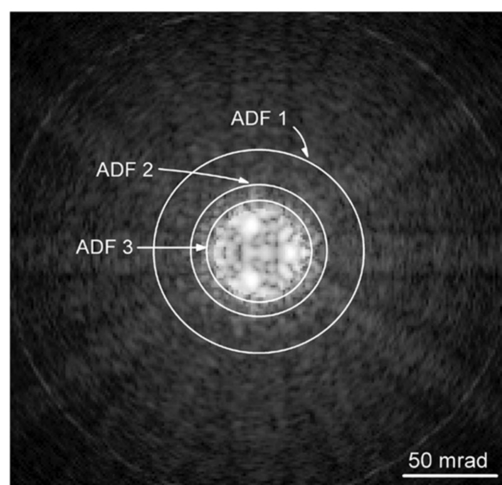

Fig. 12. Calculated CBED pattern for a 250 Å-thick Si specimen along the [1 1 0] orientation using an aberration-corrected 0.8 Å STEM probe with a 25 mrad convergence angle. The inner angles of all three ADF detector geometries are indicated on the image with white circles. The values of the detector inner angles are 54 mrad (ADF1), 35 mrad (ADF2) and 27 mrad (ADF3).

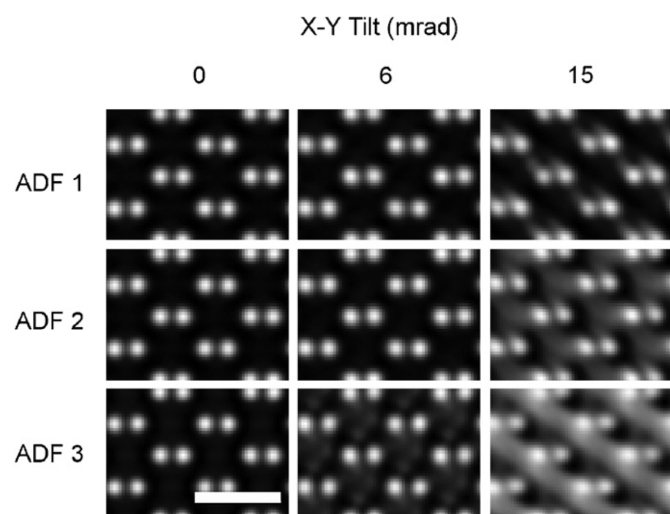

Fig. 13. Simulated ADF-STEM images of 250 Å-thick crystal silicon specimens with different tilt angles and ADF detector geometries: 54–330 (ADF1), 34–220 (ADF2) and 27–160 mrad (ADF3) inner and outer detector angles. The 0.8 Å probe was used and the crystal was tilted around the [1 1 0] crystallographic orientation. The specimen tilt angles along the x- and y-axes are indicated. All images are scaled to fill the available grayscale. The scale bar is 5 Å.

scattered electrons. To study the effects these different collection angles can have upon tilted samples, ADF images with three different ADF collector configurations were simulated. In addition to the ADF detector geometry used earlier in the paper (54–330 mrad inner–outer angles), which will be labeled ADF1 in this section, two other ADF detector geometries, ADF2 and ADF3, were simulated as well. ADF2 corresponds to 35–220 mrad inner–outer angles and ADF3 corresponds to 27–165 mrad inner–outer angles. Fig. 12 shows a calculated CBED pattern from a Si specimen aligned with the incident beam along the [1 1 0] orientation using an aberration-corrected 0.8 Å probe whose convergence angle is $\alpha_{obj} = 25$ mrad. The positions of the inner angles of all three ADF detectors used in this paper are also marked as white circles.

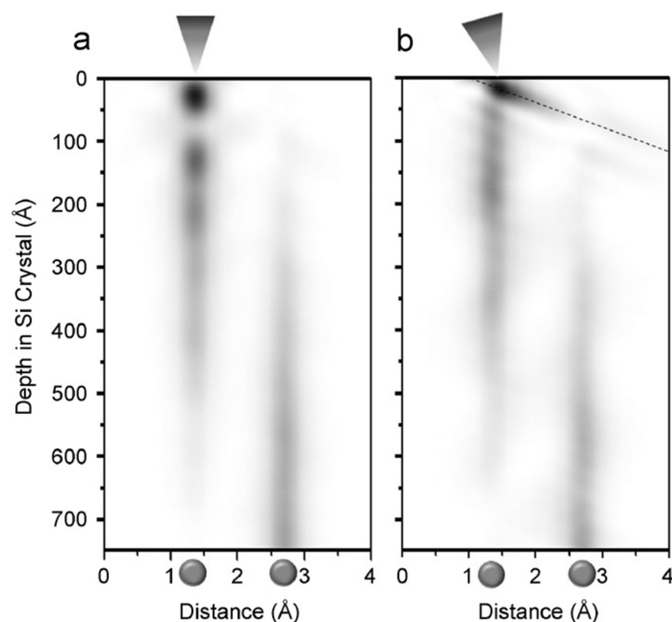

Fig. 14. Calculated intensity of the incident beam as it propagates through 750 Å of Si along the [1 1 0] orientation. An aberration-corrected 0.8 Å probe was used. The probe was located on the left-hand column of the dumbbell and the linescans are taken along the length of the dumbbell. The positions of the columns are indicated as dots below the graph: (a) for untilted and (b) for (15,0) mrad tilted specimens. Highest electron intensity is black.

To maximize the visibility of the effects of tilt, 6 and 15 mrad tilts (in both the x- and y-directions) were considered. A 250 Å thick Si crystal in the [1 1 0] orientation was used in these calculations. Here the images were simulated only for the aberration-corrected 0.8 Å STEM probe, and are presented in Fig. 13. As can be seen from this set of images, at zero-tilt the differences between different detectors are not significant. However, for a tilt of 15 mrad the images recorded with the two ADF detectors with smaller inner angles show quite visible differences in the images as compared to those calculated for the ADF1 detector. A noticeable brightening of the area between the columns is observed. Indeed, the smaller the detector inner angle the more intensity appears between the columns as the sample is tilted off-axis. This likely is caused by redistribution of the intensities in the diffracted beams and the geometry of the overlap of the CBED discs inside a particular ADF detector.

4. Discussion

The results of the multislice simulations on crystalline Si presented in the previous sections show that high-resolution ADF-STEM imaging is still possible when the sample

Author's personal copy

is slightly tilted. The effects were the same for both the uncorrected 2 Å STEM probe and the aberration-corrected 0.8 Å probe. The atomic columns of Si were quite visible up to the maximum simulated tilt of 15 mrad (or $\approx 1^{\circ}$) regardless of crystal orientation or ADF detector geometry, and remained visible for specimens as thick as 750 Å. However, the results also suggest that despite the visibility of the atomic columns the contrast in these images is expected to be reduced significantly with tilt. In the case of a 15 mrad tilt a factor of 2 reduction in contrast is predicted for all three major orientations of the crystal. Dramatic reduction of the contrast was also observed with an increase of the thickness of the specimen; from $C \simeq 4.3$ for $t = 50$ Å-thick samples to $C \simeq 2$ for $t = 450$ Å-thick samples when imaged with an aberration-corrected 0.8 Å probe.

Since the tilt of the specimen affects the strength of the channeling of the incident electrons along the atomic columns, as discussed by Loane et al. [11] the number of electrons that scatter into the ADF detector will be reduced for a tilted sample relative to the zone-axis oriented sample. Therefore, the intensity of the ADF signal at the position of the atomic columns is expected to be lower for a tilted specimen than in the non-tilted case and this is exactly what was observed in the calculations presented here. In Fig. 14 the intensity of the incident beam is calculated as a function of depth when the beam is positioned on one of the columns of the Si dumbbell along the [1 1 0] orientation. Two cases were considered: untilted and a (15,0) mrad tilt using a 0.8 Å aberration-corrected probe.

In the case of the untilted specimen strong channeling is observed (see Fig. 14(a)), which is consistent with earlier results by Hillyard et al. [23,24], Allen et al. [25] and Voyles et al. [26]. However, a significant reduction of channeling takes place when the sample is tilted off the zone axis (see Fig. 14(b)). It is interesting to note that in the case of a tilted specimen the dynamics of dechanneling of the incident probe to the neighboring column is different than in the untilted case. Less intensity is immediately channelled down the atomic column, with the remaining intensity continuing on at an angle of approx 25 mrads to the atomic column as is seen in Fig. 14(b) (along the dashed line). When the probe is located between the columns the ADF intensity is not expected to be strongly affected by the specimen tilt, since channeling is not significant at these points. This agrees with the observed relatively small changes in ADF signal for points between the columns in the simulations (see Figs. 4 and 7).

The observed dependence of the ADF signal upon the thickness of the sample is quite interesting. An early report by Hillyard and Silcox [27] based on multislice simulations performed on untilted crystals indicates that the intensity of the ADF signal from the atomic columns should increase with thicker specimens. Similar dependence is also observed in this study, even in the presence of a 15 mrad tilt. However, despite the increase of the intensities in the ADF images on-column and off-column, as can be seen in Fig. 10, the overall contrast of the image reduces corresponding to the reduction of beam channeling [11].

ADF-STEM image calculations performed for different ADF detectors indicate that the appearance of images recorded with smaller detector inner angles are more sensitive to tilt than HAADF images. In a previous study done with tilted silicon samples Yu et al. [12] showed that multislice predicted that the intensity from a column of atoms in the ADF image decreases more rapidly in HAADF detectors than LAADF detectors. This is consistent with the results of the intensity values from the columns in ADF simulated images presented here. This present study is also able to observe the intensity changes in every location in the crystal as a sample is tilted. What is observed in these images is an increased level of intensity between the columns as the angle of the ADF detector decreases. With smaller inner angles of the ADF detector the contributions of the diffracted beams become more influential in the formation of the image. When the sample is tilted, the distribution of intensities between the central disc and the diffracted discs changes, directly affecting the number of electrons collected by each ADF detector and, therefore, the intensity distribution of the ADF image. This is exactly what was observed in the simulated images presented in the previous section.

5. Conclusion

In conclusion, the results of the multislice simulations of the ADF-STEM images performed on crystalline Si using both uncorrected and aberration-corrected probes suggest:

1. Small tilts, even on the order of 10–15 mrad, can reduce the contrast of high-resolution images of the crystal by as much as a factor of 2.
2. Contrast reduction in ADF-STEM images is expected to be similar for both aberration-corrected and uncorrected probes. A factor of 2 reduction of contrast in high-resolution images is predicted for a Si crystal tilted off-axis by 15 mrad in both x- and y-axes.
3. This strong reduction of contrast with crystal tilt holds for different orientations of the crystal.
4. The thicker the sample, the more the contrast is reduced, though the rate of contrast reduction is not linear with thickness.
5. ADF detectors with smaller inner angle are more sensitive to the effects of tilt than HAADF and can be used to detect small tilts during STEM operation.

There are likely similar effects in conventional bright field TEM, which might help to clarify the "Stobbs factor".

Acknowledgments

This work is supported by the Nanoscale Science and Engineering Initiative of the NSF EEC-0117770 and NYSTAR C-020071.

Author's personal copy

References

[1] M. Haider, S. Uhlmann, E. Schhwan, H. Ross, B. Kabius, K. Urban, Nature 392 (1998) 768.
[2] P.E. Batson, O.L. Krivanek, N. Dellby, Nature 418 (2002) 617.
[3] P.D. Nellist, M.F. Chisholm, N. Dellby, O.L. Krivanek, M.F. Murffit, Z.S. Szilagyi, A.R. Lupini, A. Borisevich, W.H. Sides, S.J. Pennycook, Science 305 (2004) 1741.
[4] K.A. Mkhoyan, P.E. Batson, J. Cha, W.J. Schaff, J. Silcox, Science 312 (2006) 1354.
[5] C. Boothroyd, W.M. Stobbs, Ultramicroscopy 26 (1988) 361;
C. Boothroyd, W.M. Stobbs, Ultramicroscopy 31 (1989) 259.
[6] C. Boothroyd, J. Microscopy 190 (1997) 99.
[7] C. Boothroyd, Ultramicroscopy 83 (2000) 159.
[8] R.F. Loane, P. Xu, J. Silcox, Acta. Cryst. A47 (1991) 267.
[9] P. Xu, R.F. Loane, J. Silcox, Ultramicroscopy 38 (1991) 127.
[10] K.A. Mkhoyan, S.E. Maccagnano-Zacher, M.G. Thomas, J. Silcox, Phys. Rev. Lett, to appear.
[11] R.F. Loane, E.J. Kirkland, J. Silcox, Acta. Cryst. A 44 (1988) 912.
[12] Z. Yu, D.A. Muller, J. Silcox, Ultramicroscopy, 2007, in press, doi:10.1016/j.ultramic.2007.08.007.
[13] T. Plamann, M.J. Hytch, Ultramicroscopy 78 (1999) 153.
[14] T. Yamazaki, M. Kawasaki, K. Watanabe, I. Hashimoto, M. Shiojiri, Ultramicroscopy 92 (2002) 181.
[15] P. Wang, A.L. Bleloch, U. Falke, P.J. Goodhew, Ultramicroscopy 106 (2006) 277.
[16] J.M. Cowley, A.F. Moodie, Acta. Cryst. 10 (1957) 609.
[17] R.F. Loane, P. Xu, J. Silcox, Ultramicroscopy 40 (1992) 121.
[18] S. Hillyard, J. Silcox, Ultramicroscopy 52 (1993) 325.
[19] K.A. Mkhoyan, E.J. Kirkland, J. Silcox, E.S. Alldredge, J. Appl. Phys. 96 (2004) 738.
[20] E.J. Kirkland, Advanced Computing in Electron Microscopy, Plenum Press, New York, 1998.
[21] K.A. Mkhoyan, S.E. Maccagnano-Zacher, E.J. Kirkland, J. Silcox, Ultramicroscopy, submitted for publication.
[22] D.A. Muller, N. Nakagawa, A. Ohtomo, G.L. Grazul, H.Y. Hwang, Nature 430 (2004) 657.
[23] S. Hillyard, R.F. Loane, J. Silcox, Ultramicroscopy 49 (1995) 6.
[24] S. Hillyard, J. Silcox, Ultramicroscopy 58 (1993) 14.
[25] L.J. Allen, S.D. Findlay, M.P. Oxley, C.J. Rossouw, Ultramicroscopy 96 (2003) 47.
[26] P.M. Voyles, D.A. Muller, E.J. Kirkland, Microsc. Microanalysis 10 (2004) 291.
[27] S. Hillyard, J. Silcox, Mater. Res. Soc. Symp. Proc. 332 (1994) 361.